Experimental Brain Research (2021) 239:1165–1178
https://doi.org/10.1007/s00221-021-06036-5

RESEARCH ARTICLE

Resting fMRI-guided TMS results in subcortical and brain network modulation indexed by interleaved TMS/fMRI

Desmond J. Oathes[1] · Jared P. Zimmerman[1,2] · Romain Duprat[1] · Seda S. Japp[1] · Morgan Scully[1] · Benjamin M. Rosenberg[3] · Matthew W. Flounders[1] · Hannah Long[1] · Joseph A. Deluisi[1] · Mark Elliott[4] · Gavriella Shandler[1] · Russell T. Shinohara[1,5,6] · Kristin A. Linn[1,5,6]

Received: 26 October 2020 / Accepted: 8 January 2021 / Published online: 9 February 2021

Abstract

Traditional non-invasive imaging methods describe statistical associations of functional co-activation over time. They cannot easily establish hierarchies in communication as done in non-human animals using invasive methods. Here, we interleaved functional MRI (fMRI) recordings with non-invasive transcranial magnetic stimulation (TMS) to map causal communication between the frontal cortex and subcortical target structures including the subgenual anterior cingulate cortex (sgACC) and the amygdala. Seed-based correlation maps from each participant's resting fMRI scan determined individual stimulation sites with high temporal correlation to targets for the subsequent TMS/fMRI session(s). The resulting TMS/fMRI images were transformed to quantile responses, so that regions of high-/low-quantile response corresponded to the areas of the brain with the most positive/negative evoked response relative to the global brain response. We then modeled the average quantile response for a given region (e.g., structure or network) to determine whether TMS was effective in the relative engagement of the downstream targets. Both the sgACC and amygdala were differentially influenced by TMS. Furthermore, we found that the sgACC distributed brain network was modulated in response to fMRI-guided TMS. The amygdala, but not its distributed network, also responded to TMS. Our findings suggest that individual targeting and brain response measurements reflect causal circuit mapping to the sgACC and amygdala in humans. These results set the stage to further map circuits in the brain and link circuit pathway integrity to clinical intervention outcomes, especially when the intervention targets specific pathways and networks as is possible with TMS.

Keywords TMS · fMRI · Neuroimaging · Anxiety · Depression

Introduction

Resting fMRI seed-based connectivity is a standard approach for summarizing brain networks that are putatively functionally linked and thought to subserve treatment induced changes in affective and mental operations. Our recent work suggests that evoking activity with transcranial magnetic stimulation (TMS) to surface accessible nodes of intrinsic brain networks largely recapitulates within- and between-network correlation maps (Chen et al. 2013). Emerging approaches in fMRI connectivity promote the use of individual topographic maps before aggregating group data; this

Communicated by Francesco Lacquaniti.

✉ Desmond J. Oathes
oathes@pennmedicine.upenn.edu

[1] Department of Psychiatry, Center for Neuromodulation in Depression and Stress, University of Pennsylvania Perelman School of Medicine, Philadelphia, PA 19104, USA

[2] Department of Neuroscience, University of Pennsylvania Perelman School of Medicine, Philadelphia 19104, USA

[3] Department of Psychology, University of California Los Angeles, Los Angeles, CA 90095, USA

[4] Department of Radiology, Center for Magnetic Resonance and Optical Imaging, University of Pennsylvania Perelman School of Medicine, Philadelphia, PA 19104, USA

[5] Department of Biostatistics, Epidemiology, and Informatics, Penn Statistics in Imaging and Visualization Center, University of Pennsylvania Perelman School of Medicine, Philadelphia, PA, USA

[6] Center for Biomedical Image Computing and Analytics, University of Pennsylvania Perelman School of Medicine, Philadelphia, USA

approach may more accurately capture functional landscapes that are spatially variable across individuals but reproducible within individuals (Braga and Buckner 2017; Bijsterbosch et al. 2018). Clinically, this approach may be valuable in understanding patient idiopathic processes and treatment outcomes. In the present study, we approached individualization in brain stimulation with respect to determination of the stimulation location. Surface accessible locations were individualized using each participant's resting fMRI scan by seeding subcortical regions of interest and mapping frontal cortical areas of highest time-series correlation with the target for that individual, i.e., 'resting fMRI-guided TMS'.

The current investigation focused on stimulation accessible regions of frontal cortex hypothesized to influence deep brain structures related to affective disturbance: the amygdala and the sgACC. The amygdala is essential to a range of emotional processes and is known to be dysregulated in affective disorders such as posttraumatic stress disorder, social phobia, and depression (Etkin and Wager 2007; Hamilton et al. 2012). A large body of neuroimaging work has identified frontal regions thought to potentially regulate amygdala activity (Buhle et al. 2014; Kohn et al. 2014) and also reliably dysfunctional in clinical populations (Zilverstand et al. 2016). In a variety of non-human primate studies, amygdala functional connectivity studies in humans, and diffusion tractography studies, multiple subregions of prefrontal cortex stand out as potential targets by which TMS might causally influence the amygdala (Ghashghaei et al. 2007; Lehman et al. 2011; Neubert et al. 2015; Shiba et al. 2016; Folloni et al. 2019).

The importance of the sgACC is highlighted by many neuroimaging studies of clinical depression, a recent resting fMRI meta-analysis of MDD, as well as imaging acquired during negative mood inductions (Liotti et al. 2000; Greicius et al. 2007; Kragel and LaBar 2016; Rolls et al. 2019). In the clinical domain, when repetitive TMS treatment is delivered to regions of prefrontal cortex with higher magnitude resting time-series correlation with sgACC, the treatment tends to work more effectively (Fox et al. 2012; Weigand et al. 2018a; Cash et al. 2019). However, the neuroimaging, clinical TMS, and animal studies do not clearly prove that there are prefrontal cortical locations that causally influence the amygdala or sgACC in humans. In one recent report of dorsolateral prefrontal cortex stimulation with interleaved fMRI, there was one subject who was shown to have a clear sgACC response to TMS though generally in the other participants, the sgACC did not respond (Vink et al. 2018). This data point motivates a more sensitive individualized targeting strategy to determine a reliable sgACC modulator.

In contrast to our previous work using atlas-based targeting (Chen et al. 2013), here, we determined individual brain stimulation sites from each participant's resting fMRI scan used as a basis for subsequent interleaved TMS/fMRI scans. This approach capitalizes on work that suggests network representations in the brain are highly individual, as well as recent evidence that different networks may exist at the same anatomical location across subjects (Gordon et al. 2017). To test for the possibility that a targeted approach might on average engage the sgACC and amygdala, we interleaved single pulses of TMS with fMRI recordings which, given the slow rise time of the BOLD signal in response to an 'event' (here a single TMS pulse), allows a brain-wide causal activation map to be defined for a surface brain stimulation target. This is achieved by probing the accessible cortical site and measuring fMRI BOLD signal downstream in response to stimulation. In this work, we use the term 'causal' to refer to the evoked fMRI BOLD activation map. We acknowledge that a limitation of this initial feasibility study is that without a sham TMS control condition, the evoked response may be conflated with BOLD changes attributable to auditory and other sensory stimuli. In light of this limitation, we performed a variety of sensitivity analyses to explore the degree to which these nuisance signals may have affected the findings.

There is justification for looking at the sgACC and amygdala regions individually, though the distributed networks of both regions likely contribute to complex mental operations subserving emotion and its dysregulation in affective illness. Separate network masks for the sgACC and amygdala were generated using our processing pipeline applied to an independent healthy cohort from a publicly available source [Nathan Kline Institute-Rockland Sample (NKI)].

Previous work used individual quantile ranks in cortical thickness and resting fMRI signal amplitude to assess age-specific topological abnormalities (Chen et al. 2015). In the current study, our primary outcome was a transformation of the individual's interleaved TMS/fMRI contrast image to a quantile image, which, to our knowledge, has not been previously reported. The motivation for using quantile images was based on interest in the relative distribution of TMS-evoked brain activation as a basis for effective individualized targeting of brain networks and systems. That is, we care less about the magnitude of sgACC (de)activation relative to other individuals than whether the sgACC was one of the most (de)activated regions within the individual, relative to the response in the rest of their brain. Coupled with this individual-focused primary outcome, the individualized targeting approach in this work has direct clinical application as a basis for personalized medicine.

By including multiple stimulation sites for each subcortical target (Fig. 1), we sought to determine whether resting fMRI targeted TMS is effective generally, rather than confined to a particular subregion of frontal cortex. Our priority was to establish the feasibility of resting fMRI-guided TMS

according to the degree to which the downstream target was modulated. Similarly, we aimed to establish the degree to which distributed networks derived from those seed maps responded to TMS.

Materials and methods

Sampling strategy

Among sites accessible to TMS while participants laid supine in the scanner, we considered areas of left frontal cortex with high resting connectivity to subcortical targets of interest as stimulation sites. There were multiple sites for each participant for each target (each at least 1.47 cm apart and none within 2 cm of another stimulation site immediately preceding or following it in sequence). The number of sites that were stimulated and included for analysis varied across participants due to scanner/subject availability. This preliminary study utilized a convenience sample to test a number of targeting approaches (mostly included in this dataset) and there was no systematic reason for including more sites/sessions per participant other than convenience. For each participant, across 1–2 interleaved TMS/fMRI sessions, we stimulated multiple accessible sites for the sgACC and amygdala (see Fig. 1). Targets alternated, so that the sgACC and amygdala stimulation sites were never run sequentially.

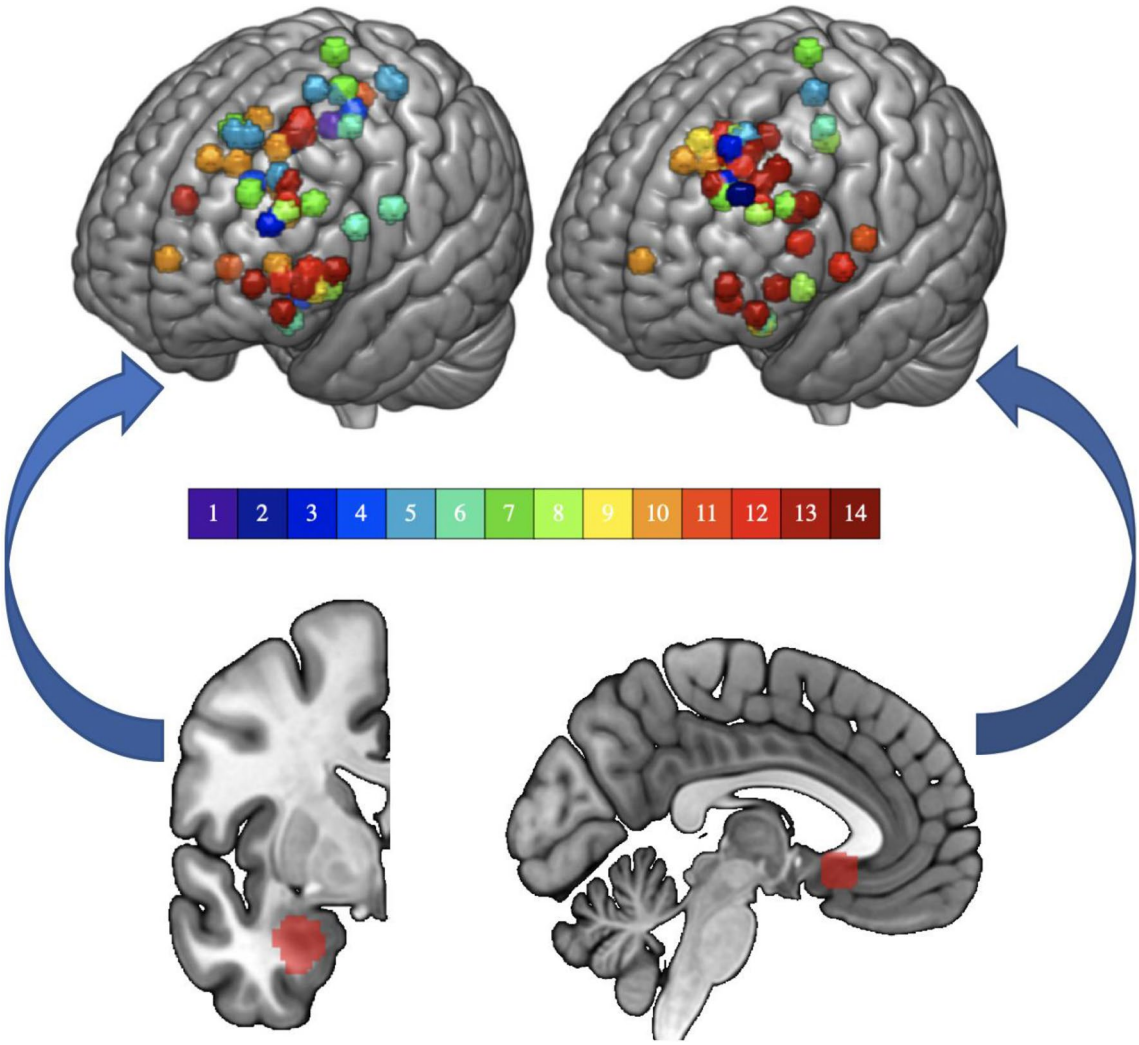

Fig. 1 Sites of stimulation and downstream targets. **a** Stimulation sites (top) based on resting fMRI seeded from the subcortical region below it (bottom). On the left, the basolateral amygdala (BLA) and on the right, the subgenual anterior cingulate cortex (sgACC). Color bar represents subject number. The sgACC is displayed at MNI $x = -4$ and the left BLA is displayed at MNI $y = -2$

Experimental design

Participants were screened to determine eligibility (see below) and then had a baseline MRI scan that was used to generate brain stimulation sites for the subsequent interleaved TMS/fMRI session(s).

Participants and sessions

All participants gave consent for the experiment according to the Declaration of Helsinki and the study was approved by the University of Pennsylvania IRB. Participants ranged from age 22 to 42 (mean 28.71, standard deviation 4.95); had Bachelor's to Doctoral education; had no history of a neurological or psychiatric condition; and were not taking any psychoactive medications. There were eight male and six female participants. In total, 72 interleaved TMS/fMRI datasets (sites) were acquired across 1–2 sessions and 4–14 runs per individual. These included 44 runs for the amygdala target and 41 runs for the sgACC (i.e., some targets had high connectivity to both targets).

Equipment

MRI data were acquired on a 3 T Siemens Prisma scanner using one head coil for baseline resting and structural MRI (64 channel; Erlangen, Germany) and another for interleaved TMS/fMRI (RAPID quad T/R single channel; Rimpar, Germany) to accommodate the custom-built TMS coil holder and TMS coil. TMS was delivered using an MRI compatible Magventure MRI-B91 air-cooled TMS coil connected to a Magpro X100 stimulator (Magventure; Farum, Denmark). Neuronavigation through a stereotaxic system (Brainsight; Rogue Research, Montreal, Quebec, Canada) matching fiduciary points from the participant with MRI images through a Polaris optical position Vicra camera allowed marking the stimulation sites on a lycra swim cap. Though we are not able to watch in real time whether the TMS coil is in place during an MRI acquisition, we take many steps to secure a tight connection in the scanner, to monitor the coil position, while the participant moves into the bore, and check immediately after each fMRI acquisition that the coil remained securely attached to the scalp target. The location for each site was based on individual functional connectivity values over which the TMS coil was placed in the MRI. A dedicated Windows PC installed with E-prime 2.0 (Psychology Software Tools, Sharpsburg, PA, USA) was used to gate TMS pulse delivery as well as MRI scans between pulses that each were triggered via TTL pulses through a parallel port with unique pin assignments for each device.

Baseline MRI acquisition

For each subject, a resting-state fMRI scan with phase-encoding direction anterior-to-posterior was acquired (TR = 720 ms, TE = 37 ms, FA = 52°, FOV = 208 mm, 2 × 2 × 2 mm voxels, 72 interleaved axial slices with no gap, 600 measurements). For that sequence, participants were instructed to keep their eyes open and remain as still as possible while staring at a central fixation (white cross on black background). Structural data were also acquired and consisted of a high-resolution multi-echo T1-weighted MPR image (TR = 2400 ms, TI = 1060 ms, TE = 2.24 ms, FA = 8°, 0.8 × 0.8 × 0.8 mm voxels, FOV = 256 mm, PAT mode GRAPPA, and 208 slices).

TMS/fMRI data

Interleaved TMS/fMRI images were acquired with an effective TR of 2400 ms (including a 400 ms gap for TMS before the subsequent volume) using a TE of 30 ms (FA = 75°, FOV = 192 mm, 3 × 3 × 4 mm voxels, 32 interleaved axial slices, and 175 measurements) in an AP phase-encoding direction. Each MRI volume acquisition was gated by TTL triggers from E-prime with a 400 ms gap between volumes to allow interleaved TMS pulses to be delivered halfway through the gap (at 200 ms). This avoids known magnetic field contamination by simultaneous MRI acquisition during TMS pulse delivery, but, given the slow BOLD signal rise time, effectively captures TMS-evoked brain responses. Single pulses were interleaved in 12 mini-blocks of seven stimulations separated by 1 TR and including 0, 1, or 2 'catch trials' (random order and block) during which spacing was separated by an extra TR with no TMS pulse to avoid easy prediction of TMS delivery by participants (Fig. 2). The mini-blocks were themselves separated by 7 TRs and 72 total stimulations were given per site over 175 volume acquisitions.

MRI processing

For processing resting fMRI data, the first 10 volumes were discarded for T1 equilibrium, and then an automated removal of motion artifact designed to maintain fMRI autocorrelation structure using ICA-AROMA (Pruim et al. 2015) was applied. Nuisance regression, residualizing for white matter and CSF signal, was implemented in FSL 5.08 (FMRIB Oxford, UK), followed by band-pass filtering 0.008–0.1 Hz and 6 mm kernel FWHM smoothing. Boundary-based registration following FSL FAST tissue segmentation used six degrees of freedom to coregister T1 to functional scans and FSL FNIRT default settings were used for nonlinear warps of fMRI data to the 2 mm MNI152 average template. The inverse of this process moved seed regions to native fMRI

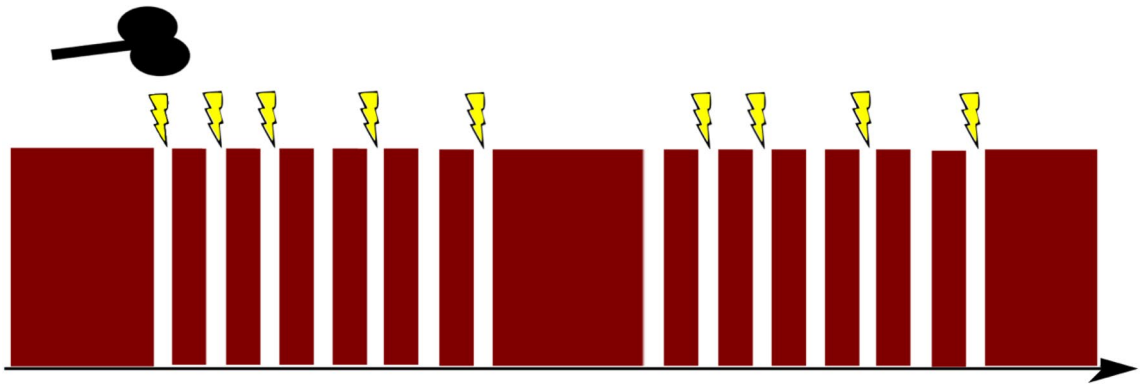

Fig. 2 TMS/fMRI interleaved mini-blocks. TMS single pulses were interleaved with fMRI recordings with as few as one TR (thin red vertical segments) separating TMS pulses (lightning bolts) in each of 12 mini-blocks. Two sample mini-blocks are included in the figure along with representations of randomly spaced catch trials (no lightning bolt) to reduce participants' ability to predict TMS onsets

space in one step, and functional connectivity for each seed was calculated in native space, resulting in Pearson correlation maps that were transformed to z scores using the Fisher's r-to-z equation. Inverting the T1 to functional transform placed the fMRI connectivity maps in native T1 space for neuronavigation that were also visually verified. TMS/fMRI data analysis removed two initial volumes for T1 equilibrium and then regressed TMS events convolved with a hemodynamic response function (SPM12 double gamma) on the fMRI time-series with regressors of no interest and six motion parameters derived from FSL MCFLIRT motion correction. The resulting contrast estimates were subjected to additional analysis and statistical procedures described below.

TMS site determination

For both sgACC and amygdala targets, resting functional connectivity (FC) z score values of absolute value 0.15 or greater were considered for targeting. For the amygdala, FC was, on average, mean (sd) $z = 0.5(0.19)$ with a range 0.15–0.84. For the sgACC, we had an average mean (sd) $z = 0.48(0.18)$ with a range 0.22–0.86. This threshold was based on early qualitative assessments that found multiple frontal sites at the brain surface for TMS targeting in every participant, optimizing generalizability of the approach. For some sites, FC values for both targets exceeded this threshold and so were included in both sgACC and amygdala analyses (see overlapping spheres in Fig. 1). For sgACC targets, seven had negative FC values with the sgACC, and for amygdala targets, six had negative FC values with the amygdala. For both the sgACC and BLA, the responses corresponding to the negatively correlated sites were similar to the positively correlated sites (see the Results section of the Supplementary Materials). Positive FC sites were easier to find and more numerous, but also were prioritized given evidence that electrical stimulation of the brain is more robust for positive FC sites (Keller et al. 2011). However, given the precedent that negative FC targeting for the sgACC is showing promising results (Fox et al. 2012; Weigand et al. 2018b; Cash et al. 2019, 2020a; Cole et al. 2020), we chose to include negative FC targets.

The FDI (first dorsal interosseous) or APB (abductor pollicis brevis) of the participant's right (dominant) hand was used (whichever most clearly responded) as target muscles for determining motor threshold based on visual observation (5/10 trials with a noticeable resting muscle twitch). Stimulation intensity was then set to 120% resting-motor threshold for all stimulation delivered to that participant. The TMS coil was positioned on each stimulation site with the coil handle facing backwards for a posterior-to-anterior-induced current. This maintained consistency and allowed the TMS coil to be reliably fit in the MRI head coil over each site though also precluded a more optimized position considering gyral orientation.

The sgACC seed was based on an average major depressive disorder (MDD) associated abnormality across 14 neuroimaging studies and shown to change in connectivity following rTMS treatment (Liston et al. 2014) positioned just to the left of midline ipsilateral to the stimulation sites and also anatomically well centered to Brodmann 25 (16 mm diameter sphere) at MNI -2, 18, -8 (Fig. 1 bottom right). Inverting the normalization warp to native space was confirmed visually for each subject to be anatomically consistent with sgACC. The BLA seed (Fig. 1 bottom left) was defined using a probability map with threshold 40% for the BLA from a common histological atlas (Amunts et al. 2005), and voxels were retained only if they exceeded the probability threshold for adjoining subregions (centromedial amygdala, CMA; superficial amygdala, SF).

The gray matter mask was based on visual confirmation using FSL version 5.0.8 with an arbitrary value of '100' + (scaled probability/245) based on visual inspection of the 152 average T1 gray matter tissue prior in standard space.

In each TMS-fMRI session, the TMS coil was placed on the scalp at a location determined immediately prior to the scan in a TMS neuronavigation session to target frontal sites with strong functional connectivity to either the amygdala or sgACC. The large diameter MRI head coil and custom-built TMS coil holder allowed access to all a priori determined frontal sites though occasionally requiring participants to slightly tilt their heads to accommodate the apparatus.

Network masks and FreeSurfer ROIs

An independent resting fMRI and structural T1 database were used to define normative atlases for each of the amygdala (Fig. 3) and sgACC (Fig. 4) seed regions (see the Network Mask and FreeSurfer ROIs sections of the Supplementary Materials for details). FreeSurfer masks (Fig. S3) for the amygdala and sgACC (Fischl et al. 2002; Destrieux et al. 2010; Fischl 2012), though not used to define stimulation sites, were used as ROIs and seeds for FC maps (Figs. 3, 4) to test the specificity or generalizability of the findings.

Statistical methods

TMS-induced fMRI activation was assessed with a traditional first-level GLM analysis with models including the TMS pulse blocks and six motion parameters from FSL MCFLIRT. Contrast estimates from the TMS-evoked fMRI data demonstrated non-comparable levels of variability across participants (Fig. S2), which motivated our transformation of the contrasts to within-scan quantiles before performing group-level tests (see Sect. 1A. of the Supplementary Materials for additional details).

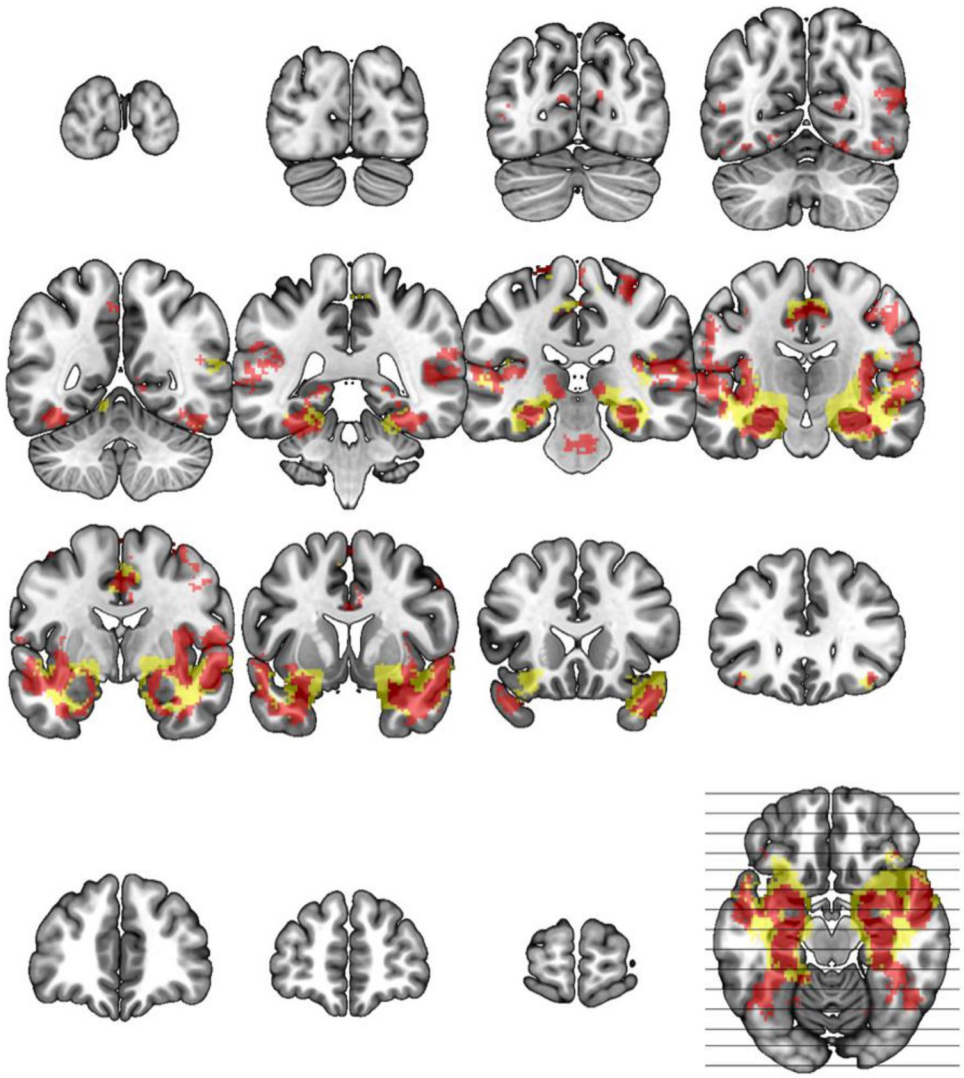

Fig. 3 Basolateral and full amygdala network. Using an independent data set, the network mask shown was created seeding the BLA (red) or FreeSurfer amygdala (yellow) defined regions of interest and calculating functional connectivity (correlation) with $z \geq 0.3$ in 96 + /127 subjects, effect size > 6.0 and cluster ≥ 2 mm^3 in 2 mm MNI standard space (excluding seed). Slice wise views are represented starting at MNI $y = -98$ and moving forward in 12 mm steps until the final $y = 66$ image

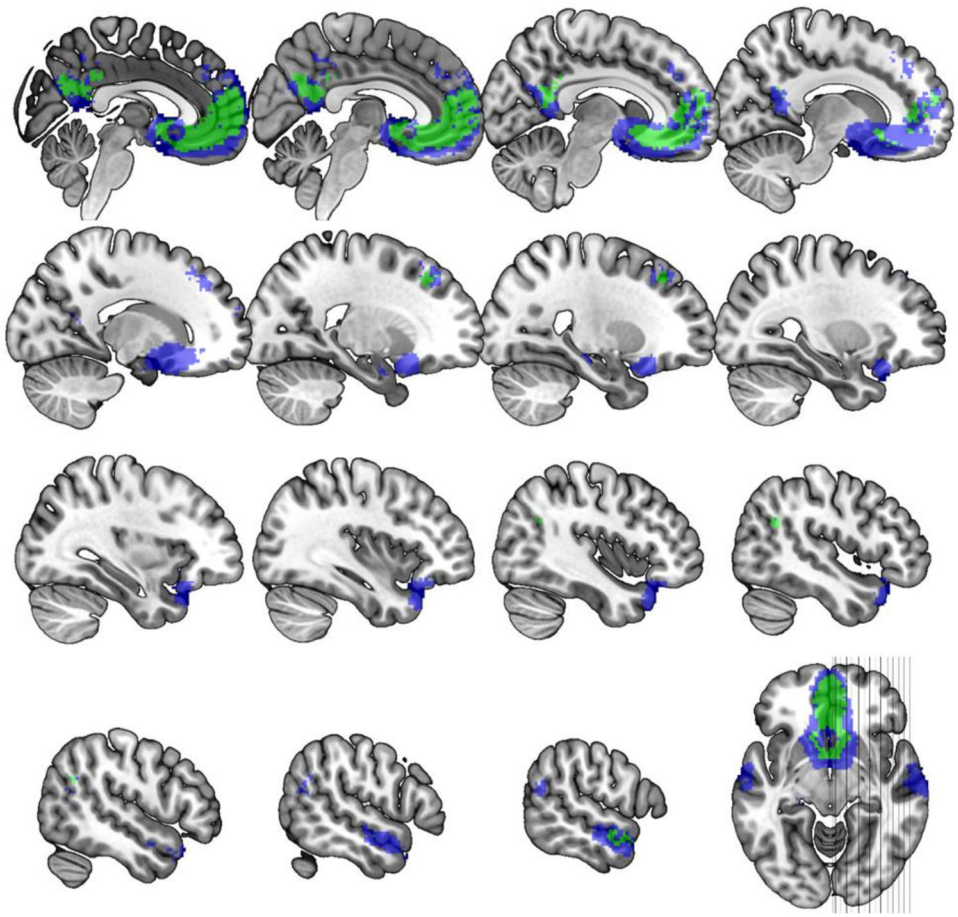

Fig. 4 Subgenual cingulate network. Using an independent data set, the network mask shown was created seeding the primary (green) or FreeSurfer (blue) defined sgACC and calculating functional connectivity (correlation) with $z \geq 0.3$ in 96 + /127 subjects, effect size > 6.0 and cluster ≥ 2 mm^3 in 2 mm MNI standard space (excluding seed). Slice wise views are represented starting at MNI $x = 2$ and moving out in 2 mm steps with an extra step between rows until the final $x = 58$ image

Group-level analyses were performed using generalized estimating equations (GEE), a semi-parametric extension of general linear models for non-independent data. We calculated the average quantile response within a region of interest (ROI) for each image and then centered these values by 0.5, so that the sign of the intercept parameter estimate in the GEE model would correspond to greater than or less than the median response, which we found approximately corresponded to positive and negative response values for the region, respectively (see Fig. S1).

We fit GEEs with an exchangeable working correlation structure for each ROI with the average quantile response as the outcome. All models controlled for age, head motion (mean absolute value of root-mean-squared, six degrees of freedom calculated with fMRI image realignment), and resting functional connectivity between the stimulation site and target (which by definition were restricted to only high values; see Sect. II of the Supplementary Materials for resting fMRI connectivity analyses). GEEs model the population average response for given values of the model covariates. We therefore centered all covariates, so that the intercept corresponded to the average response for a population with average values of the covariates.

Finally, we performed an exploratory voxel-wise analysis using the 44 amygdala target quantile images. We fit a GEE at every voxel (within the amygdala subregion mask) to account for repeated-measures within subject. The voxel-wise GEE models adjusted for age, head motion, and pain ratings.

Data and code sharing

Data are available from the first author by request following a formal data sharing agreement. Analysis code not already included in R packages will be shared freely via Github upon request of the senior author.

Results

To simplify exposition of the results, we will refer to the response, which is the quantile TMS-evoked response averaged within an ROI at the individual image level, as simply 'the response'. Model-based results will refer to the average response (average referring to across subjects) accounting for repeated-measures within subjects. Supplementary Table 1 displays parameter estimates, standard errors, test

statistics, p values, and effect sizes from all primary tests presented in Sects. 3.1, 3.2. Supplementary Fig. 1 also demonstrates individual subject TMS-evoked response data using fMRI contrast estimates before conversion to quantiles. These averages are consistent with directionality labels in the quantile analyses and demonstrate how individual data points contributed to model summaries.

Amygdala and subgenual cingulate targeted TMS influenced proposed target regions

We used the basolateral amygdala (BLA) as a seed to target frontal stimulation but anticipated that interconnected subregions of the amygdala might have also responded to TMS given their proximity and reciprocal functional connections. When testing the ipsilateral BLA, we did not establish evidence for an activated (i.e., greater than median) average response, with a liberal, ≥ 30% BLA probability mask from histological maps (Amunts et al. 2005) (Fig. 5; parameter estimate (PE) = 0.006, Wald $\chi^2 = 0.02$, $p = 0.875$). Employing a smaller 50% BLA map did not change the findings (PE = 0.007, Wald $\chi^2 = 0.03$, $p = 0.858$). In the centromedial (CMA) and superficial (SF) amygdala, we found a significant activated average response in both subregions (Fig. 5; CMA 30% PE = 0.055, Wald $\chi^2 = 5.22$, $p = 0.022$; SF 30% PE = 0.062, Wald $\chi^2 = 4.19$, $p = 0.041$), suggesting that specific subregions are influenced by this amygdala targeted TMS approach. Using an independent amygdala ROI (see Fig. S3) from the Harvard–Oxford subcortical atlas (Fischl et al. 2002) yielded parameter estimates in the same direction that were not significant (left amygdala PE = 0.036, Wald $\chi^2 = 1.03$, $p = 0.310$; full amygdala PE = 0.034, Wald $\chi^2 = 1.29$, $p = 0.257$).

The average sgACC region response was significant and negative following targeted TMS (Fig. 5; PE = − 0.061, Wald $\chi^2 = 3.98$, $p = 0.046$). Dilating the mask by 1 voxel (2 mm space; spherical kernel) slightly weakened the strength of the association (PE = − 0.057, Wald $\chi^2 = 3.74$, $p = 0.053$), suggesting that the targeted region, and not the adjacent cortical space, was particularly affected by TMS. Using an independent (Fig. S3) surface-based atlas for the sgACC (Destrieux et al. 2010), we found a negative PE (− 0.038) that did not exceed the significance threshold (Wald $\chi^2 = 2.80$, $p = 0.094$). It is noteworthy that both sgACC masks are in close proximity to a medial prefrontal canonical DMN subregion which prompted additional exploratory analyses that excluded DMN voxels when calculating the response variable (see the Results section in the Supplementary Materials). We found that the results were robust to the choice of working correlation structure for the GEE models (see Sect. II in the Supplementary Materials).

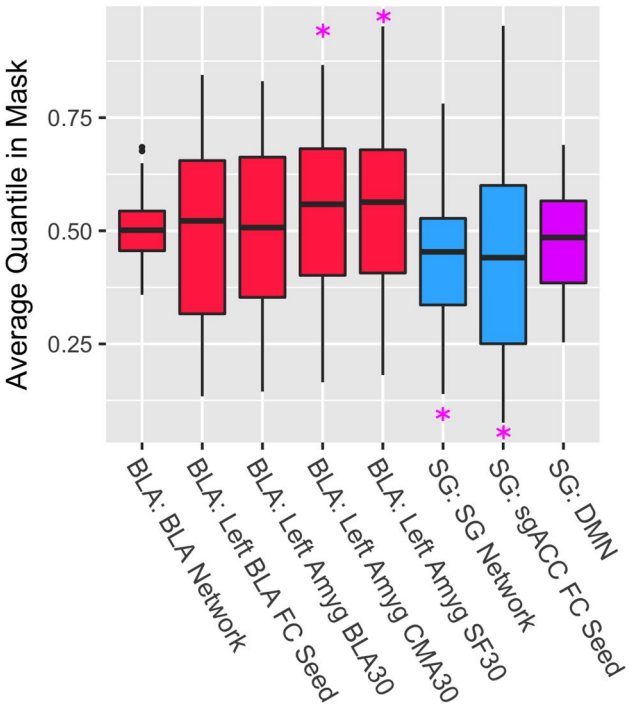

Fig. 5 Distribution of Quantile TMS response averaged within ROIs. fMRI-guided TMS evokes brain responses in downstream subcortical targets including the amygdala and subgenual anterior cingulate cortex. Solid lines in the bars represent the median and the box hinges are the 25th and 75th percentiles. Whiskers are at the min/max but no further than 1.5* IQR (interquartile range). An average quantile response in an ROI mask that is less than 0.5 represents 'lower' than median TMS-evoked response for that particular scan for that individual. Similarly, values greater than 0.5 represent 'higher' than within-individual, within-session median-evoked TMS response. 'BLA' and 'SG' labels before the colon represent the stimulation target of Basolateral Amygdala or Subgenual cingulate. 'FC' seeds are the primary regions of interest; 'Networks' represent the networks from independent FC based atlases. '30' represents 30 + % probability from a histological atlas. 'CMA' and 'SF' are centromedial and superficial amygdala, respectively. '*' indicates $p < .05$ significance based on the GEE model that controlled for age, motion, and functional connectivity between the stimulation site and target

Network-level responses to TMS

The average sgACC network response was strong and negative (PE = − 0.059, Wald $\chi^2 = 21.20$, $p = 0.000004$; Fig. 5), but the BLA network response was not significant ($p = 0.439$; for additional details and an analysis using alternative network maps, see the Supplementary Materials).

The sgACC network largely overlaps with the canonical DMN (Fig. S4), particularly in the ventromedial prefrontal cortex. We therefore conducted sensitivity analyses to investigate the specificity of the sgACC network result with respect to DMN response. These analyses demonstrated that the negative sgACC network response persisted even when the DMN was excluded from the network mask, indicating

that the results were not driven by the DMN. Details are given in Sect. II of the Supplementary materials.

Exploratory voxel-wise analyses

Given that the BLA was used as a target, but the TMS-evoked effects were most pronounced in the CMA and SF subregions (not in the BLA target), we performed an exploratory voxel-wise analysis to better characterize the actual location of the largest average response. We hypothesized that there might be evidence of some degree of BLA engagement given that this was our intended target. Due to the inapplicability of standard cluster-extent thresholding or permutation testing with our use of GEE at each voxel, we adjusted for multiple testing using a false discovery rate of $q < 0.05$ within a mask that included all three subregions (partially overlapping) each at a 30% + threshold. The peak corrected voxel in that mask was at MNI x,y,z (− 20, − 6, − 12), $q < 0.0001$, with the following histology-based probabilities: 78% superficial, 68% laterobasal, and 56% centromedial (Fig. 6). In other words, the amygdala subregions were all well represented in the peak average amygdala response.

Wald statistical maps from the voxel-wise GEE analyses (separately for BLA and sgACC targets) are included in Supplementary Figs. S5, S6. Areas with large Wald statistics demonstrate partial overlap with the sgACC and BLA networks defined using the independent atlas.

Gyral region of stimulation site is associated with amygdala response

The stimulation sites were grouped using Desikan atlas parcels that included the inferior frontal gyrus (IFG; pars opercularis, triangularis, and orbitalis together), the superior frontal gyrus (SFG), precentral gyrus (PCG), and medial-frontal gyrus (MFG; rostral + caudal together) regions, as demonstrated in Fig. S7.

For the sgACC, the brain region effect on average response was not significant (df = 3, Wald $\chi^2 = 0.88$, $p = 0.831$) and the smallest p value for pairwise brain region comparisons was 0.23. Similarly, for the sgACC network, there was not a significant brain region effect (df = 3, Wald $\chi^2 = 3.61$, $p = 0.307$, and the smallest p value for the pairwise regional comparisons was 0.10).

Among the amygdala regions, there was a main effect of brain region on left BLA response (df = 3, Wald $\chi^2 = 46.2$, $p < 0.0001$) driven especially by the IFG inducing a significantly lower response than the MFG and SFG (PE = 0.112, Wald $\chi^2 = 6.51$, $p = 0.011$; PE = 0.139, Wald $\chi^2 = 9.94$, $p = 0.0002$) as well as PCG lower than MFG and SFG (PE = 0.236, Wald $\chi^2 = 7.38$, $p = 0.007$; PE = 0.263, Wald $\chi^2 = 8.18$, $p = 0.004$). Neither MFG and SFG nor PCG and IFG were significantly different from one another (PE = 0.027, Wald $\chi^2 = 0.76$, $p = 0.383$; PE = 0.124, Wald $\chi^2 = 2.42$, $p = 0.200$). Neither the CMA nor SF responses differed significantly by brain region (df = 3, Wald $\chi^2 = 3.46$, $p = 0.326$; df = 3, Wald $\chi^2 = 2.452$, $p = 0.484$). Likewise, the amygdala (BLA) network response was not significantly associated with the particular brain region stimulated (df = 3, Wald $\chi^2 = 2.30$, $p = 0.513$). In Supplementary Fig. 7, we illustrate that there are cortical regions that when stimulated modulated the amygdala in a negative direction (BLA in response to IFG and PCG TMS; CMA in response to PCG TMS) which is the putatively clinically useful direction.

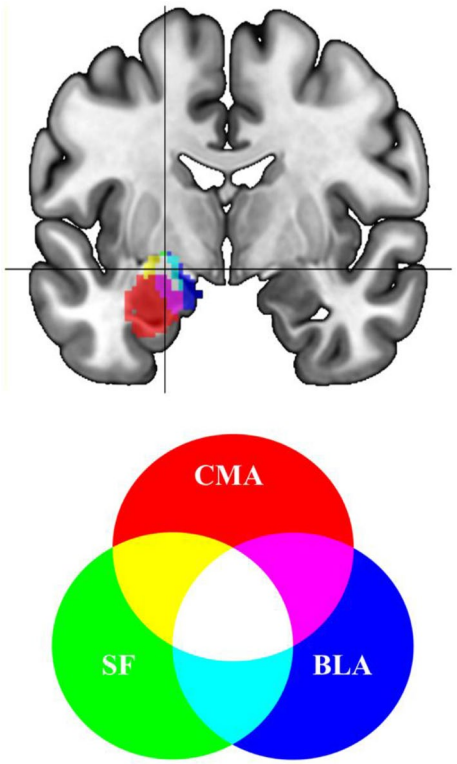

Fig. 6 Peak amygdala response to TMS. In a combined basolateral (blue), centromedial (red), and superficial (green) amygdala volume, the peak average response (FDR corrected; $p < .05$) at MNI xyz (− 20, − 6, − 12) is indicated by the crosshairs and represents a coordinate with 78% SF, 68% BLA and 56% CMA probability based on an histology generated atlas

Sensitivity analyses

This proof of concept study did not include a control site which is the typical benchmark for measuring TMS-induced effects. Therefore, we performed a number of sensitivity analyses to assess the robustness of the primary results and quantify the effects of other potential influencing factors.

Specificity of the average TMS responses

TMS induces a scalp sensation and a noticeable auditory stimulus even in the noisy MRI environment with earplugs in place. This general TMS effect causes a related brain change [e.g., (Siebner et al. 1999)] that we attempted to mitigate here using three strategies. Running new models adjusting for TMS-evoked responses in somato-motor areas (Yeo et al. 2011), masking out overlaps in our networks with the somato-motor areas, and masking out overlaps between the somato-motor areas and an average TMS-evoked map across all sites did not qualitatively change the results (see Sect. II of the Supplementary Materials).

Effects of cortical distance

Given that each stimulation site was not exactly the same distance from the scalp, the 'dose' of TMS delivered to the brain might differ across sites and influence the TMS-evoked response. We found that distance did influence evoked responses but only for amygdala targets (details in the Results section of the Supplementary Materials).

Effects of pain/discomfort

Adjusting for pain/discomfort ratings as an additional covariate in the models had little effect on the results qualitatively (see the Results section of the Supplementary Materials).

Effects of physiological arousal

Physiological arousal was generally not associated with the average response (see Sect. II of the Supplementary Materials), with the exception of the sgACC. Despite the significant association between physiological arousal and sgACC response, the overall average response in the sgACC remained negative and significant in the model that included physiological arousal (see Sect. II of the Supplementary Materials).

Evoked response and baseline FC

None of the subregion or network-evoked responses were correlated with resting FC at baseline (see Supplementary Materials, Sect. II) with the exception of the sgACC response that was positively correlated with baseline FC. Future studies with a wider range of FC values should explore whether this relationship holds.

Responses in the target region and network are correlated

The relationship between the sgACC region and its network was supported by a positive Pearson correlation between the response in the sgACC and the response in the sgACC network ($r = 0.482$; $p = 0.001$) (Fig. S8). The same positive relationship was observed between the responses in the amygdala and amygdala network ($r = 0.505$; $p = 0.0004$) (Fig. S8). Though the amygdala network was not significantly modulated by TMS, this correlation further links networks to individual ROI target-evoked responses to TMS. To the extent that neuropsychiatric patients have pathologies characterized by network abnormalities, these findings set the stage for integrating brain networks connected to ROI targets as outcome measures in neuromodulation intervention studies.

Discussion

In this investigation, we provide the first evidence that individualized resting fMRI-guided TMS can indirectly and noninvasively modulate targeted subcortical areas and their distributed network representations. TMS treatments are delivered to single brain areas, but their clinical effects are not likely confined to the stimulation site at the cortical surface. In support for targeted approaches to brain stimulation, we establish here the use of TMS to target the subgenual anterior cingulate cortex (sgACC) and amygdala via frontal stimulation sites. We have established the use of interleaved TMS/fMRI for validating canonical resting-state brain networks (Chen et al. 2013) that we build upon by demonstrating that the sgACC as well as the distributed functional network with which it is connected respond to individualized sgACC targeted TMS. The amygdala response peak was in a zone where several subregions of the amygdala complex overlap as determined by a human histological atlas (Amunts et al. 2005). The amygdala responded to targeted TMS, while the distributed amygdala network was not effectively engaged.

Binning by gyral region added preliminary suggestions on selecting among high FC targets: the medial-frontal and superior-frontal zones were the best amygdala activators, whereas the precentral gyrus and inferior frontal gyrus/ventrolateral prefrontal cortex decreased basolateral amygdala quantile TMS response. Since decreasing amygdala response is putatively the preferred clinical direction, this finding suggests the IFG/vlPFC and PCG as new targets for neuromodulation. The sgACC and its network yielded negative responses regardless of specific cortical region. Given the lack of FC strength related to BLA, BLA network, or sgACC network responses to TMS as well as the positive

association between resting functional connectivity and the sgACC response to TMS, the use of resting FC to guide TMS should not place undue emphasis on relative FC values in deciding on a target. Rather, a reasonable cutoff of 'high FC' should be used to guide targeting any variety of cortical zones for the sgACC. Cortical distance was strongly associated with amygdala responses to TMS but not associated with the sgACC or its network response. Thus, choosing sites close to the scalp or increasing stimulation intensity for amygdala targets further from the scalp is supported by our results.

In this investigation of resting fMRI-guided TMS targeting, the precise targeting location varied by individual as did each subject's TMS-evoked brain map that was ranked voxel-wise by magnitude to obtain a quantile image before being aggregated across subjects for sgACC or amygdala target analyses. In the behavioral domain, it has been demonstrated that individual functional localization is better than anatomical localization which is better than a group functional template, which is better than a scalp EEG coordinate in terms of effect size influences on behavior (Sack et al. 2009). Using a common anatomical target in the prefrontal cortex has been shown to generate highly variable individual sgACC responses in TMS/fMRI readouts (Vink et al. 2018). Clinically, using an atlas-based stimulation site for the sgACC also does not result in superior outcomes for treatment of depression compared with a standard scalp measurement-based target (O'Reardon et al. 2007; Blumberger et al. 2018). In contrast, there are multiple studies now, showing that resting connectivity between the stimulation site and the sgACC predict treatment response (Fox et al. 2012; Weigand et al. 2018a; Cash et al. 2019) and that prospective sgACC FC targeting leads to depression improvement (Cole et al. 2020). Though we did not explicitly test our targeting approach against an atlas-based method, individual targeting was effective here in modulating the intended downstream targets. Our results are consistent with preliminary findings in the TMS literature and support recent cognitive neuroscience work that observes individually specific functional network mapping (Braga and Buckner 2017; Bijsterbosch et al. 2018).

TMS targeting was done using mostly positively correlated prefrontal sites with subcortical targets of interest. Nevertheless, the stimulation sites differed in the direction of induced quantile BOLD response with the amygdala target resulting on average in a greater than median quantile BOLD response and the sgACC resulting in a less than median quantile BOLD response, which roughly corresponded to positive and negative BOLD responses, respectively (see Fig. S1). This occurred despite having overlapping sites that were stimulated for the sgACC and amygdala. The hemodynamic response to TMS likely depends on a number of factors including the degree to which inhibitory interneurons are activated (Di Lazzaro and Ziemann 2013), whether the induced field is strong enough to activate synapses in addition to axons (Attwell and Laughlin 2001) and also the brain state at the time of stimulation (Allen et al. 2007). Mapping negative and positive functional connectivity targets is also controversial, and does not indicate necessarily an excitatory or inhibitory pathway especially in the context of brain stimulation (Keller et al. 2011). The strength of single TMS pulses can be influenced by the brain state during mental states such as motor imagery (Oathes et al. 2008) or anxiety (Oathes et al. 2008). Manipulating and/or measuring brain state during TMS will add additional understanding to the conditions favoring specific directional changes in BOLD response. Similarly, in a more-balanced negative and positive FC dataset, comparing modulation for positively and negatively correlated sites will be useful to determine their differential effectiveness. Though the DLPFC has been a traditional target for TMS treatment studies, our findings do not support this region as a uniquely efficacious modulator. Better powered comparison studies will be needed to determine if this region has any special significance as a treatment target.

Our discovery of positive correlations between TMS-evoked responses in specific targeted regions of interest and their distributed networks further supports our contention that TMS is effective in targeting not only individual targeted downstream regions but also brain networks by activating individual network nodes in surface accessible stimulation sites (Chen et al. 2013). On a related note, TMS shows promise for validating causal models derived from other imaging modalities such as resting fMRI and diffusion MRI that are the basis for our current understanding of how brain networks communicate (Reid et al. 2019).

Most results were robust to variations in heart rate or respiration recorded during interleaved TMS/fMRI runs. One exception was the respiration relationship with the sgACC response. Although this relationship is interesting and it is worth examining whether respiratory changes are related to clinical response to TMS, the sgACC response to TMS remained significant in the model that included physiological arousal, suggesting that the sgACC response to TMS is not fully explained by these influences.

Limitations in the present proof of concept study included a relatively small number of participants (though a large number of stimulation sites across participants). Also, though the sgACC network response was not driven by the DMN response to TMS, the sgACC ROI and sgACC network at least partially covaried with the DMN response. As a result, the DMN response to TMS could contribute mechanistically to, for example, repetitive TMS (rTMS) treatment in depression shown to alter sgACC–DMN connectivity (Liston et al. 2014). Though we took pains to account for non-specific TMS effects on fMRI signals, the gold standard

comparison for TMS is to compare active with sham stimulation or a control site which should be a focus of future studies. Our work sheds light on a targeting approach for administering TMS to engage the sgACC and amygdala. This approach is best described as 'circuit mapping' and 'target engagement' that will hopefully lead to a wider variety of clinical, behavioral, and basic studies (Oathes et al. in press). The reliability of resting fMRI (Noble et al. 2019) calls into question whether this tool is robust and sufficient to guide TMS targeting in the clinic (Fox et al. 2013; Cash et al. 2020b). This is related to but also partially independent of whether TMS/fMRI mapping captures clinically useful information. The mapping approach also does not define the degree to which targeted circuits are modifiable using rTMS or other interventions. Further optimization for TMS pulse shape, amplitude and number of stimulations, pulse train frequency, and brain state contributions to neural and clinical effects should be explored in addition to spatial target optimization. Another limitation is that here we provide only a preliminary glimpse into which cortical zones may be especially effective in modulating target regions and networks. A variety of additional imaging features could be explored as predictors of the effectiveness by which TMS engages targeted downstream brain regions.

Conclusion

In this study, we establish a proof of concept that resting fMRI-guided non-invasive brain stimulation is effective in causally modulating subcortical targets such as the subgenual anterior cingulate cortex and the amygdala. Adding to enthusiasm for individualized brain network representations, we demonstrate the result of individualizing TMS target locations for each participant through analysis of quantile values extracted from first-level GLM contrasts in TMS-evoked fMRI data. We further contend that interleaved TMS/fMRI is a powerful technique for probing causal circuit pathways that can uncover mechanistic details especially in determining how neuromodulation changes brain, behavior, and symptoms. Future research in our lab and others will establish the relevance of this type of circuit mapping approach to individual differences in response to neuromodulation targeting specific brain networks. Although this preliminary study does not provide evidence for individual selectivity among multiple potential targets, the goal to determine whether, on average, resting fMRI-guided targeting can modulate intended brain targets sets the stage for additional optimization studies for maximizing individual brain responses. This will build on work showing that baseline fMRI, symptom, and demographic variations predict clinical response to rTMS treatment (Liston et al. 2014; Drysdale et al. 2017; Weigand et al. 2018a). The ultimate goal of TMS mapping and neuromodulation studies in healthy and patient populations is to optimize neuromodulation to move the brain from a less to a more optimal state (Medaglia et al. 2017). The field of interleaved TMS/fMRI is still in its infancy and approaches to use these causal maps to investigate circuit by circuit contributions to complex behavior and neuropsychiatric conditions are worthy of focused study (Oathes et al. in press) built on basic research such as that presented here and in similar recent studies (Hanlon et al. 2016; Fonzo et al. 2017a, b).

Supplementary Information The online version contains supplementary material available at https://doi.org/10.1007/s00221-021-06036-5.

Acknowledgments We thank Dr. Yvette Sheline for contributions to this project including equipment, scan time, and personnel. We also thank Yordan Todorov of Magventure, Inc. for TMS device support and contributing customized equipment for hardware control.

Funding This work was supported by the National Institutes of Health NIH R01 MH111886 (DJO) and NIH RF1 MH116920 (DJO). The funder had no role in study design; collection and analysis of data; in writing the report; or in the decision to submit the article for publication.

Data availability Data are available from the first author upon request and following a data use agreement.

Code availability Code for analysis is already available in online repositories as described in the text.

Compliance with ethical standards

Conflict of interest There are no conflicts or competing interests from the authors.

Ethics approval All participants gave consent for the experiment according to the Declaration of Helsinki and the study was approved by the University of Pennsylvania IRB.

Consent for publication All authors agree to the publication of the results described in the manuscript.

References

Allen EA, Pasley BN, Duong T, Freeman RD (2007) Transcranial magnetic stimulation elicits coupled neural and hemodynamic consequences. Science 317:1918–1921. https://doi.org/10.1126/science.1146426

Amunts K, Kedo O, Kindler M et al (2005) Cytoarchitectonic mapping of the human amygdala, hippocampal region and entorhinal cortex: intersubject variability and probability maps. Anat Embryol 210:343–352

Attwell D, Laughlin SB (2001) An energy budget for signaling in the grey matter of the brain. J Cereb Blood Flow Metab 21:1133–1145. https://doi.org/10.1097/00004647-200110000-00001

Bijsterbosch JD, Woolrich MW, Glasser MF et al (2018) The relationship between spatial configuration and functional connectivity of brain regions. Elife 7:e32992. https://doi.org/10.7554/eLife.32992

Blumberger DM, Vila-Rodriguez F, Thorpe KE et al (2018) Effectiveness of theta burst versus high-frequency repetitive transcranial magnetic stimulation in patients with depression (THREE-D): a randomised non-inferiority trial. Lancet 391:1683–1692. https://doi.org/10.1016/s0140-6736(18)30295-2

Braga RM, Buckner RL (2017) Parallel interdigitated distributed networks within the individual estimated by intrinsic functional connectivity. Neuron 95:457-471.e455. https://doi.org/10.1016/j.neuron.2017.06.038

Buhle JT, Silvers JA, Wager TD et al (2014) Cognitive reappraisal of emotion: a meta-analysis of human neuroimaging studies. Cereb Cortex 24:2981–2990. https://doi.org/10.1093/cercor/bht154

Cash RF, Zalesky A, Thomson RH, Tian Y, Cocchi L, Fitzgerald PB (2019) Subgenual functional connectivity predicts antidepressant treatment response to transcranial magnetic stimulation: independent validation and evaluation of personalization. Biol Psychiat 86:e5–e7

Cash RF, Cocchi L, Lv J, Fitzgerald PB, Zalesky A (2020a) Functional magnetic resonance imaging–guided personalization of transcranial magnetic stimulation treatment for depression. JAMA Psychiatry

Cash RF, Weigand A, Zalesky A, Siddiqi SH, Downar J, Fitzgerald PB, Fox MD (2020b) Using brain imaging to improve spatial targeting of TMS for depression. Biol Psychiatry

Chen AC, Oathes DJ, Chang C et al (2013) Causal interactions between fronto-parietal central executive and default-mode networks in humans. Proc Natl Acad Sci U S A 110:19944–19949. https://doi.org/10.1073/pnas.1311772110

Chen H, Kelly C, Castellanos FX, He Y, Zuo XN, Reiss PT (2015) Quantile rank maps: a new tool for understanding individual brain development. Neuroimage 111:454–463. https://doi.org/10.1016/j.neuroimage.2014.12.082

Cole EJ, Stimpson KH, Bentzley BS et al (2020) Stanford accelerated intelligent neuromodulation therapy for treatment-resistant depression. Am J Psychiatry 2019:19070720

Destrieux C, Fischl B, Dale A, Halgren E (2010) Automatic parcellation of human cortical gyri and sulci using standard anatomical nomenclature. Neuroimage 53:1–15. https://doi.org/10.1016/j.neuroimage.2010.06.010

Di Lazzaro V, Ziemann U (2013) The contribution of transcranial magnetic stimulation in the functional evaluation of microcircuits in human motor cortex. Front Neural Circuits 7:18. https://doi.org/10.3389/fncir.2013.00018

Drysdale AT, Grosenick L, Downar J et al (2017) Resting-state connectivity biomarkers define neurophysiological subtypes of depression. Nat Med 23:28–38. https://doi.org/10.1038/nm.4246

Etkin A, Wager TD (2007) Functional neuroimaging of anxiety: a meta-analysis of emotional processing in PTSD, social anxiety disorder, and specific phobia. Am J Psychiatry 164:1476–1488

Fischl B, Salat DH, Busa E et al (2002) Whole brain segmentation: automated labeling of neuroanatomical structures in the human brain. Neuron 33:341–355

Fischl B (2012) FreeSurfer. Neuroimage 62:774–781. https://doi.org/10.1016/j.neuroimage.2012.01.021

Folloni D, Sallet J, Khrapitchev AA, Sibson N, Verhagen L, Mars RB (2019) Dichotomous organization of amygdala/temporal-prefrontal bundles in both humans and monkeys. Elife 8:e47175. https://doi.org/10.7554/eLife.47175

Fonzo GA, Goodkind MS, Oathes DJ et al (2017) PTSD psychotherapy outcome predicted by brain activation during emotional reactivity and regulation. Am J Psychiatry 2017:16091072

Fonzo GA, Goodkind MS, Oathes DJ et al (2017) Selective effects of psychotherapy on frontopolar cortical function in PTSD. Am J Psychiatry 2017:16091073

Fox MD, Buckner RL, White MP, Greicius MD, Pascual-Leone A (2012) Efficacy of transcranial magnetic stimulation targets for depression is related to intrinsic functional connectivity with the subgenual cingulate. Biol Psychiatry 72:595–603. https://doi.org/10.1016/j.biopsych.2012.04.028

Fox MD, Liu H, Pascual-Leone A (2013) Identification of reproducible individualized targets for treatment of depression with TMS based on intrinsic connectivity. Neuroimage 66:151–160. https://doi.org/10.1016/j.neuroimage.2012.10.082

Ghashghaei HT, Hilgetag CC, Barbas H (2007) Sequence of information processing for emotions based on the anatomic dialogue between prefrontal cortex and amygdala. Neuroimage 34:905–923. https://doi.org/10.1016/j.neuroimage.2006.09.046 (**S1053-8119(06)00989-X[pii]**)

Gordon EM, Laumann TO, Gilmore AW et al (2017) Precision functional mapping of individual human brains. Neuron 95:791-807.e797. https://doi.org/10.1016/j.neuron.2017.07.011

Greicius MD, Flores BH, Menon V et al (2007) Resting-state functional connectivity in major depression: abnormally increased contributions from subgenual cingulate cortex and thalamus. Biol Psychiatry 62:429–437. https://doi.org/10.1016/j.biopsych.2006.09.020 (**S0006-3223(06)01193-0**)

Hamilton JP, Etkin A, Furman DJ, Lemus MG, Johnson RF, Gotlib IH (2012) Functional neuroimaging of major depressive disorder: a meta-analysis and new integration of baseline activation and neural response data. Am J Psychiatry 167(3):693–703. https://doi.org/10.1176/appi.ajp.2012.11071105

Hanlon CA, Dowdle LT, Moss H, Canterberry M, George MS (2016) Mobilization of medial and lateral frontal-striatal circuits in cocaine users and controls: an interleaved TMS/BOLD functional connectivity study. Neuropsychopharmacology 41:3032–3041. https://doi.org/10.1038/npp.2016.114

Keller CJ, Bickel S, Entz L, Ulbert I, Milham MP, Kelly C, Mehta AD (2011) Intrinsic functional architecture predicts electrically evoked responses in the human brain. Proc Natl Acad Sci U S A 108:10308–10313. https://doi.org/10.1073/pnas.1019750108

Kohn N, Eickhoff SB, Scheller M, Laird AR, Fox PT, Habel U (2014) Neural network of cognitive emotion regulation—an ALE meta-analysis and MACM analysis. Neuroimage 87:345–355. https://doi.org/10.1016/j.neuroimage.2013.11.001

Kragel PA, LaBar KS (2016) Decoding the nature of emotion in the brain. Trends Cogn Sci 20:444–455. https://doi.org/10.1016/j.tics.2016.03.011

Lehman JF, Greenberg BD, McIntyre CC, Rasmussen SA, Haber SN (2011) Rules ventral prefrontal cortical axons use to reach their targets: implications for diffusion tensor imaging tractography and deep brain stimulation for psychiatric illness. J Neurosci 31:10392–10402. https://doi.org/10.1523/jneurosci.0595-11.2011

Liotti M, Mayberg HS, Brannan SK, McGinnis S, Jerabek P, Fox PT (2000) Differential limbic–cortical correlates of sadness and anxiety in healthy subjects: implications for affective disorders. Biol Psychiatry 48:30–42 (**S0006-3223(00)00874-X[pii]**)

Liston C, Chen AC, Zebley BD et al (2014) Default mode network mechanisms of transcranial magnetic stimulation in depression. Biol Psychiatry 76:517–526. https://doi.org/10.1016/j.biopsych.2014.01.023

Medaglia JD, Zurn P, Sinnott-Armstrong W, Bassett DS (2017) Mind control as a guide for the mind. Nature Human Behaviour 01:1–8

Neubert FX, Mars RB, Sallet J, Rushworth MF (2015) Connectivity reveals relationship of brain areas for reward-guided learning and decision making in human and monkey frontal cortex. Proc

Natl Acad Sci U S A 112:E2695–E2704. https://doi.org/10.1073/pnas.1410767112
Noble S, Scheinost D, Constable RT (2019) A decade of test-retest reliability of functional connectivity: a systematic review and meta-analysis. Neuroimage 203:116157
Oathes DJ, Balderston NL, Kording KP, et al. (in press) TMS/fMRI for Probing and modulating neural circuits relevant to affective disorders. WIREs Cognitive Science
Oathes DJ, Bruce JM, Nitschke JB (2008) Worry facilitates corticospinal motor response to transcranial magnetic stimulation. Depress Anxiety 25:969–976. https://doi.org/10.1002/da.20445
O'Reardon JP, Solvason HB, Janicak PG et al (2007) Efficacy and safety of transcranial magnetic stimulation in the acute treatment of major depression: a multisite randomized controlled trial. Biol Psychiatry 62:1208–1216. https://doi.org/10.1016/j.biopsych.2007.01.018
Pruim RHR, Mennes M, van Rooij D, Llera A, Buitelaar JK, Beckmann CF (2015) ICA-AROMA: A robust ICA-based strategy for removing motion artifacts from fMRI data. Neuroimage 112:267–277. https://doi.org/10.1016/j.neuroimage.2015.02.064
Reid AT, Headley DB, Mill RD et al (2019) Advancing functional connectivity research from association to causation. Nat Neurosci 22:1751–1760. https://doi.org/10.1038/s41593-019-0510-4
Rolls ET, Cheng W, Gong W et al (2019) Functional connectivity of the anterior cingulate cortex in depression and in health. Cereb Cortex 29:3617–3630. https://doi.org/10.1093/cercor/bhy236
Sack AT, Cohen Kadosh R, Schuhmann T, Moerel M, Walsh V, Goebel R (2009) Optimizing functional accuracy of TMS in cognitive studies: a comparison of methods. J Cogn Neurosci 21:207–221. https://doi.org/10.1162/jocn.2009.21126
Shiba Y, Santangelo AM, Roberts AC (2016) Beyond the medial regions of prefrontal cortex in the regulation of fear and anxiety. Front Syst Neurosci 10:12. https://doi.org/10.3389/fnsys.2016.00012
Siebner HR, Peller M, Willoch F et al (1999) Imaging functional activation of the auditory cortex during focal repetitive transcranial magnetic stimulation of the primary motor cortex in normal subjects. Neurosci Lett 270:37–40. https://doi.org/10.1016/s0304-3940(99)00454-1
Vink JJT, Mandija S, Petrov PI, van den Berg CAT, Sommer IEC, Neggers SFW (2018) A novel concurrent TMS-fMRI method to reveal propagation patterns of prefrontal magnetic brain stimulation. Hum Brain Mapp 39:4580–4592. https://doi.org/10.1002/hbm.24307
Weigand A, Horn A, Caballero R et al (2018) Prospective validation that subgenual connectivity predicts antidepressant efficacy of transcranial magnetic stimulation sites. Biol Psychiatry 84:28–37. https://doi.org/10.1016/j.biopsych.2017.10.028
Weigand A, Horn A, Caballero R et al (2018) Prospective validation that subgenual connectivity predicts antidepressant efficacy of transcranial magnetic stimulation sites. Biol Psychiat 84:28–37
Yeo BT, Krienen FM, Sepulcre J et al (2011) The organization of the human cerebral cortex estimated by intrinsic functional connectivity. J Neurophysiol 106:1125–1165. https://doi.org/10.1152/jn.00338.2011
Zilverstand A, Parvaz MA, Goldstein RZ (2016) Neuroimaging cognitive reappraisal in clinical populations to define neural targets for enhancing emotion regulation. A systematic review. Neuroimage 151:105–116. https://doi.org/10.1016/j.neuroimage.2016.06.009